In situ X-ray diffraction study of reduction processes of Fe_3O_4- and $Fe_{1−x}O$-based ammonia-synthesis catalysts

Yi-Fan Zheng [a,b,*], Hua-Zhang Liu [a,b], Zong-Jian Liu [a,b], Xiao-Nian Li [a,b]

[a] *College of Chemical Engineering and Materials Science, Zhejiang University of Technology, Hangzhou 310014, PR China*
[b] *Catalysis Institute, Zhejiang University of Technology, Hangzhou 310014, PR China*

ABSTRACT

The temperature-programmed reduction process of two types of industrial ammonia-synthesis catalysts, A110 and ZA-5, which are, respectively, based on Fe_3O_4 and $Fe_{1−x}O$ precursors, were studied by *in situ* X-ray power diffraction (XRD). It has been found that the ZA-5 has lower reduction temperature and faster reduction rate, and its active phase α-Fe possesses a higher value of lattice microstrain than A110. The simulation based on Rietveld refinement has also shown that the shape of α-Fe grain of ZA-5 has a mixed shape of cube and sphere with more exposing (111) and (211) planes, while that of A110 looks like a concave cube with more exposing (110) planes. Based on the results obtained, a growth model of α-Fe during the reduction of Fe_3O_4- and $Fe_{1−x}O$-based ammonia-synthesis catalysts is proposed, and the origins for the activity difference has been also discussed.

© 2009 Elsevier Inc. All rights reserved.

1. Introduction

The iron-based catalysts have been the subject of intense studying in recent years because of its wide applications in various fields, such as ammonia synthesis [1–4], water–gas shift reaction [5] and Fischer–Tropsch synthesis [6]. For ammonia synthesis, the early iron-based catalysts are obtained from magnetite, and a well-known mode describing these Fe_3O_4-based catalysts were proposed by Fagherazzi et al. [7]. Later, a new type of catalysts, namely the $Fe_{1−x}O$-based ammonia synthesis catalysts (e.g. A301 and ZA-5) were invented by our group [8], which show much higher activity and lower reduction temperature than the traditional Fe_3O_4-based catalysts and have recently also drawn increasing attention [1,9]. Pernicone et al. [1] found that the higher activity of $Fe_{1−x}O$-based ammonia synthesis catalysts, with respect to those obtained from magnetite, is related to the higher efficiency of Fe surface sites in the activation of dinitrogen and the highly dispersed Ca oxide plays decisive role in this mechanism. However, despite the well-done work by Pernicone et al. [1] and our previous studies on the possible reasons for the difference in catalytic activity between two types of catalysts [10–12], a microstructurally comprehensive study of $Fe_{1−x}O$- and Fe_3O_4-based catalysts has not been reported. It is well known that the catalytic activity for ammonia synthesis catalysts depends strongly on the microstructure of the active phase after reduction [13]. As a result, a comparative investigation of the microstructure evolution of the active phase α-Fe of $Fe_{1−x}O$- and Fe_3O_4-based catalysts during the activation process might be crucial to our understanding of the origins for the activity difference. In our early work, the reduction of two types of catalysts was examined step-by-step at which the sample was taken out at every step after cooling in the air. Such an *ex situ* study not only generates errors resulting from instrument itself and sample preparation, but also cannot exhibit the real evolution of microstructure and phase transformation of fused-iron based catalysts during reduction.

In this article we report our experimental investigation of the temperature-programmed reduction processes of two commercial catalysts, Fe_3O_4-based A110 and $Fe_{1−x}O$-based ZA-5, in a reactor appended to X-ray diffractometer (XRD) at the conditions similar to the industrial activation process. The advantages of this *in situ* XRD experiment, compared to *ex situ*, are obvious: exactly the same part of the sample is studied during the whole reduction process, and no heating-up and cooling-down procedures are needed. The purpose of this work is two-fold. First, by using this *in situ* XRD experiment the growth mode of the active phase α-Fe in fused-iron based catalysts will be examined. Second, the origins for the activity difference between $Fe_{1−x}O$- and Fe_3O_4-based catalysts will also be addressed.

2. Experimental

The commercial catalysts A110 and ZA-5 were obtained from Catalyst Factory of Zhejiang University of Technology. The main chemical compositions of A110 and ZA-5 are, respectively,

* Corresponding author at: College of Chemical Engineering and Materials Science, Zhejiang University of Technology, Hangzhou 310014, P.R.China. Fax: +86 571 88320961.
E-mail address: zhengyifan@zjut.edu.cn (Y.-F. Zheng).

Fe_3O_4–Al_2O_3–K_2O–CaO and $Fe_{1-x}O$–Al_2O_3–K_2O–CaO, and the detailed information about these catalysts, e.g. chemical compositions and pore structures, can be found in our early studies [8,10–12]. For both catalysts the activity test was carried out at a pressure of 15 MPa with a space velocity of $3 \times 10^4\,h^{-1}$. The mixed gas (N_2:$H_2 = 1$:3) is obtained by decomposition of ammonia.

X-ray diffraction was performed with a Thermo ARL X'TRA diffractometer using Cu-$K\alpha$ radiation, which is equipped with Si (Li) solid detector at 45 KV/40 mA without monochromator. The in situ experiments were carried out in Anton Paar XRK 900 reactor built in the diffractometer with a TCU 750 temperature control unit. The heating rate is 2 K/min, and a mixed gas (N_2:$H_2 = 1$:3), decomposed from ammonia at 0.7 MPa, passes the reactor with a flow rate of 0.5 l/min. The normal XRD patterns tracing the phase transformation are carried out in a continuous scan mode, with a step of 0.04° from 28° to 66° at a speed of 10° per minute. The detail XRD patterns used to calculate crystallite size and microstrain are carried out in the step-scanning mode, with a step of 0.02° and counting times of 1 s per step. The instrumental broadening was corrected by using an NIST 1976 (α-Al_2O_3) (Standard Reference Material from US Department of Commerce National Institute of Standard and Technology) under the same conditions as the experiment.

The XRD data acquisition and analysis in this work were carried out using WinXRD software, which is a part of the Thermo ARL X'TRA package supplied by the ARL Applied Research Laboratories S.A. The determination of the crystallite sizes, the size distribution and the lattice microstrain of the active phase α-Fe during reduction was conducted by a line-broadening analysis. The reflection broadening in the XRD patterns is attributed mainly to three kinds of contributions: crystallite size, microstrain, and the instrument itself [14,15]. Fourier transfer was used for the line profile analysis of reflections in order to separate the effect of crystallite size and microstrain on reflection broadening. In these XRD experiments, the software based on Warren–Averbach Fourier transfer (W-A/FT) method [16–18] was used to calculate the distribution of crystallite size and microstrain of α-Fe. Morphological analysis of α-Fe grain is performed on Popa model using Software Maud 2.046 [19,20]. A JEOL-2100F field emission high-resolution transmission electron microscope (FE-HRTEM) operated at 200 kV was employed to determine the size and microstructure of α-Fe.

3. Results

3.1. Comparison of catalytical activity between two types of catalysts

Fig. 1 shows the catalytical activity of two types of catalysts, A110 and ZA-5. At a given reaction temperature, the activity of ZA-5 is higher than that of A110, suggesting that $Fe_{1-x}O$-based catalyst ZA-5 is obviously more active than Fe_3O_4-based catalyst A110 in ammonia synthesis.

3.2. Reduction temperatures

The XRD patterns of two catalysts, A110 and ZA-5, as a function of reduction temperature are shown in Figs. 2 and 3, respectively. For both two catalysts, the active phase α-Fe is formed directly from the reduction of the precursor, wustite ($Fe_{1-x}O$) or magnetite (Fe_3O_4), because no other intermediate phases are observed. However, there exists obvious difference between A110 and ZA-5 catalysts in the temperatures at which the active phase α-Fe appears and the precursor vanishes. As can be seen from Fig. 2, for the FeO-based catalyst A110, the active phase α-Fe appears at
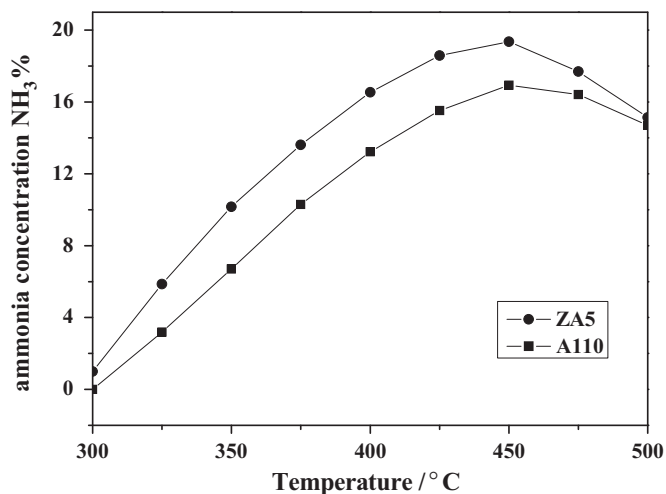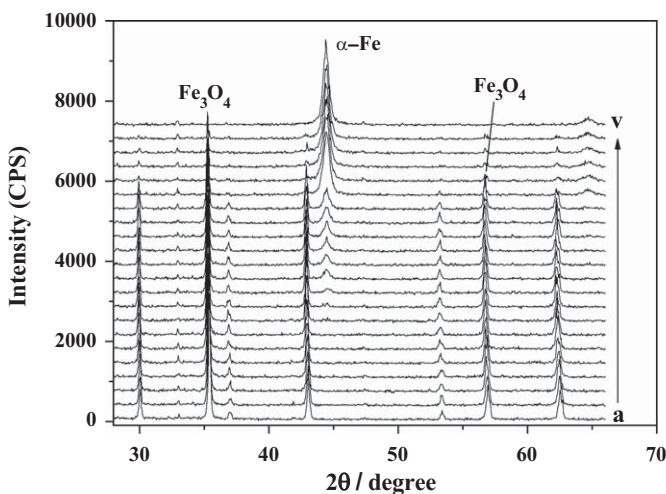

Fig. 1. Activity comparison between A110 and ZA-5.

Fig. 2. The evolution of diffraction patterns of A110 catalyst as a function of reduction temperature. Temperatures (°C): (a) 50, (b) 100, (c) 150, (d) 200, (e) 250, (f) 300, (g) 325, (h) 333, (i) 343, (j) 350, (k) 355, (l) 359, (m) 362, (n) 366, (o) 370, (p) 375, (q) 385, (r) 388, (s) 392, (t) 395, (u) 400, (v) 450.
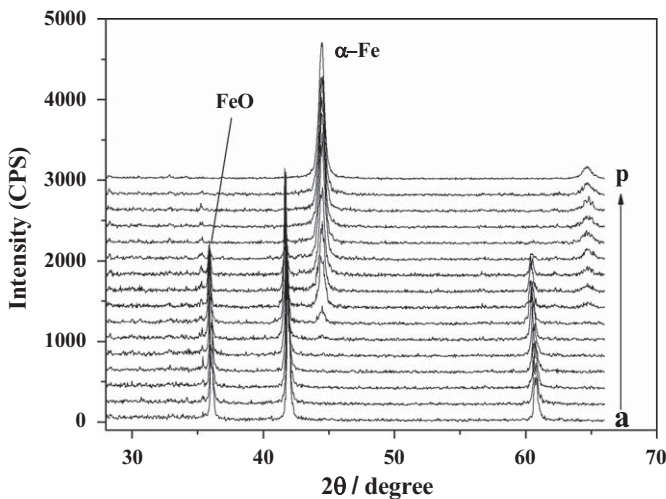

Fig. 3. The evolution of diffraction patterns of ZA-5 catalyst as a function of reduction temperature. Temperatures (°C): (a) 50, (b) 100, (c) 150, (d) 200, (e) 250, (f) 300, (g) 325, (h) 333, (i) 343, (j) 350, (k) 355, (l) 359, (m) 362, (n) 370, (o) 375, (p) 400.

about 343 °C and the precursor disappears at about 450 °C, but the corresponding temperatures for the $Fe_{1-x}O$-based catalyst ZA-5 are, respectively, 300 and 362 °C (see Fig. 3), 43 and 88 °C lower than those of the A110 catalyst. The result indicates that the $Fe_{1-x}O$-based catalyst ZA-5 has a lower reduction temperature and a faster reduction rate (namely a narrower reduction temperature range) than the Fe_3O_4-based catalyst A110. The result agrees with our early observation by conventional temperature-programmed reaction (TPR) [21].

The observation that the $Fe_{1-x}O$-based catalyst ZA-5 has a lower reduction temperature and a faster reduction rate can be attributed to the following fact: in contrast to the precursor Fe_3O_4 of a steady spinel structure [22], $Fe_{1-x}O$ is a non-stoichiometric compound with a large amount of Fe^{3+} vacancies in the crystal lattice. The presence of these cation vacancies favors the diffusion of iron ion and electron transfer ($Fe^{2+} \rightarrow O \rightarrow Fe^{3+}$) in $Fe_{1-x}O$. As a result, the precursor $Fe_{1-x}O$ is more active during reduction.

3.3. Grain growth of active phase α-Fe

For both types of catalysts, we found that the growth of α-Fe crystallites is anisotropy with preferential growth along the [110], [200] and [211] crystallographic directions with the intensities of these reflection peaks increasing with temperature (see Figs. 2–4). To further investigate the growth of α-Fe during temperature-programmed reduction, we calculated the average grain sizes of α-Fe at different temperature stages based on the intensities of these reflection peaks. Table 1 shows the average grain sizes of the active phase α-Fe during catalyst reduction. All the data of grain sizes are extracted from Scherrer formula using Scherrer Mode of WinXRD software. Two features can be found from Table 1: (i) at the beginning of reduction, the average grain sizes of α-Fe decrease with temperature, especially for A110 catalysts; (ii) with further increasing temperature, the grain sizes only slightly change with temperature. The overall evolution trend of grain size calculated from (110) reflection for ZA-5 catalyst can be more clearly seen in Fig. 5. As can be seen from Fig. 5, before the occurrence of sintering at 700 °C (namely a rapid increase in grain size), the grain size keeps relatively stable with increasing temperature. The result is probably related to the phenomenon that the exsolution products, coming from the structure promoters, segregate the grain boundaries and thus hinder grain growth [13]. Since XRD peak intensities are related to both the number and grain size of the measured materials, the above
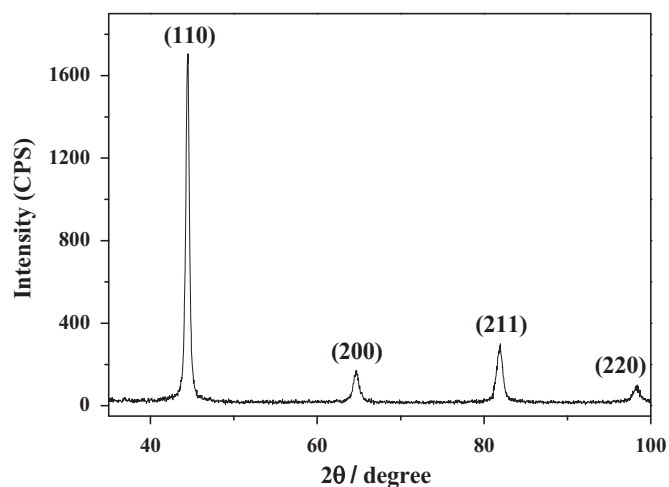

Fig. 4. Typical diffraction patterns of α-Fe for ZA-5 catalyst at a reduction temperature of 450 °C.

Table 1
Summary of average grain sizes of α-Fe during catalyst reduction.

Temp. (°C)	Catalyst					
	A110			ZA-5		
	Average grain size (nm)			Average grain size (nm)		
	(110)	(200)	(211)	(110)	(200)	(211)
325	–	–	–	18.9	11.7	13.4
350	21.6	–	–	18.2	11.0	12.2
375	17.5	9.8	12.0	18.5	12.4	13.6
400	17.6	10.9	13.7	18.3	13.8	13.1
450	17.2	10.9	13.7			
Average	18.6	10.5	13.2	18.49	12.2	13.1

All the data are extracted from Scherrer formula using Scherrer Mode of WinXRD software.
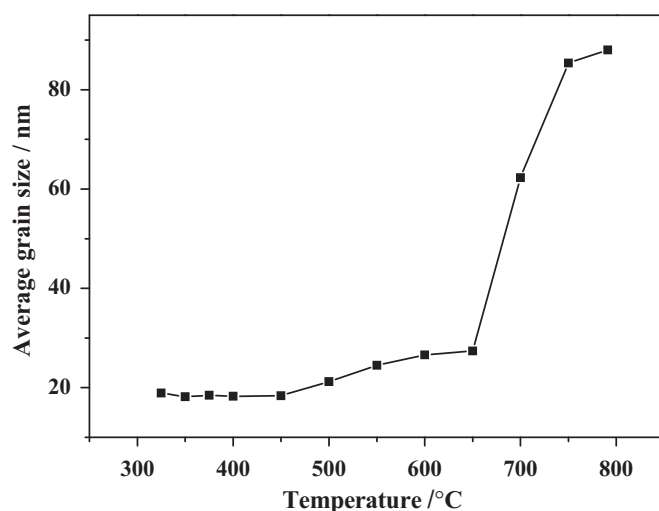

Fig. 5. The evolution of average grain size of α-Fe calculated from the (110) reflection for ZA-5 catalyst.

observation demonstrates that the observed increase in peak intensity of α-Fe with increasing temperature (see Figs. 2 and 3) is mainly related to the rise in the number of α-Fe grain.

Fig. 6 shows the evolution of lattice parameter as a function of reduction temperature during ZA-5 catalyst reduction. It should be pointed out that the evolution trend of lattice parameter as a function of reduction temperature is independent of the type of the catalyst. As can be seen from Fig. 6, the lattice parameter of α-Fe is larger than that of standard references ($a = 0.28664$ nm, JCPDS card number 19-0696). Moreover, the lattice parameter increases linearly with temperature up to 700 °C. This result is related to the fact that the XRD patterns are collected under in situ conditions where the high temperature can result in the lattice expansion. However, when the temperature reaches 700 °C, a decrease in lattice parameter is observed. This phenomenon might be attributed to the rapid sintering of α-Fe at high temperatures where the lattice expansion is hindered by the rapid grain growth.

3.4. Size distribution and microstrain analysis of active phase α-Fe

Since the Scherrer formula neglects the contribution of microstrain to the grain size, to further confirm the results mentioned above, the line profile analysis of Fe (110) reflections were also analyzed by Warren–Averbach's method. Table 2 shows
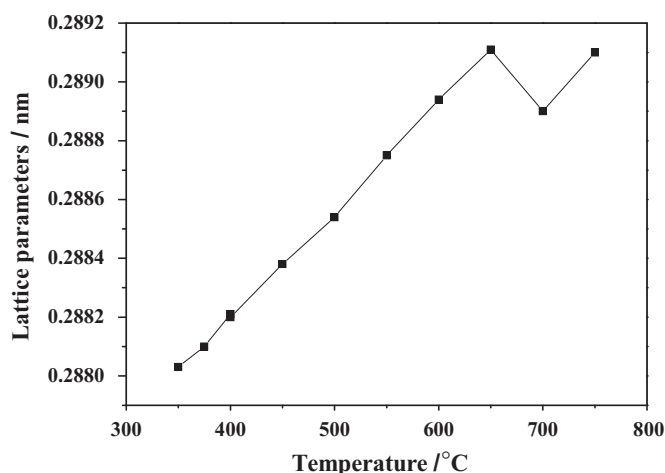
Fig. 6. The evolution of lattice parameter of α-Fe for ZA-5 catalyst as a function of reduction temperature.

Table 2
Summary of the average grain sizes and mircostrain of α-Fe during catalyst reduction calculated by Warren–Averbach method.

Temp. (°C)	Catalyst					
	A110			ZA-5		
	Average grain size (nm)	Difference with Sherrer method (nm)	Microstrain	Average grain size (nm)	Difference with Sherrer method (nm)	Microstrain
325	–	–	–	14.3	4.6	0.0026
350	18.0	3.6	0.0020	14.2	4.0	0.0024
375	14.8	2.7	0.0021	15.0	3.5	0.0023
400	15.5	2.1	0.0017	15.0	3.3	0.0020
450	15.9	1.3	0.0016			

Fig. 7. Size distribution of active phase α-Fe at different reduction temperatures for (a) A110 and (b) ZA-5.

the average grain sizes and microstrain of α-Fe for both A110 and ZA-5 catalysts calculated using Warren–Averbach's analysis. The difference in average grain size coming from two different analytical methods is also shown in Table 2. The size distribution of the active phase α-Fe at different temperatures can be observed in Fig. 7. As can be seen from Table 2, despite the presence of the difference in average grain size between two methods, the general trend of α-Fe grain size with temperature is the same as that found in Table 1. From Fig. 7, it can be also found that the grain size distribution becomes wider with increasing temperature, especially for ZA-5. Moreover, because the difference in average grain size obtained by using Scherrer formula and Warren–Averbach's method is an indication of the contribution of lattice microstrain, the larger difference observed at lower temperatures suggest that lattice microstrain is larger at the beginning of reduction. The evolution trend of microstrain with temperature can be seen from Fig. 8. In general, larger microstrain is observed at lower temperatures, especially for ZA-5 catalyst where a decrease trend in microstrain with increasing temperature can be observed. In addition, we can also find that lattice microstrain decreases with grain size from Fig. 8. These evolution features can be found in both ZA-5 and A110. However, a comparison in microstrain between two types of catalysts reveals that at different temperatures α-Fe of ZA-5 catalyst in general possess a higher value of lattice microstrain than that of A110 catalyst. The larger microstrain existing in active phase of the
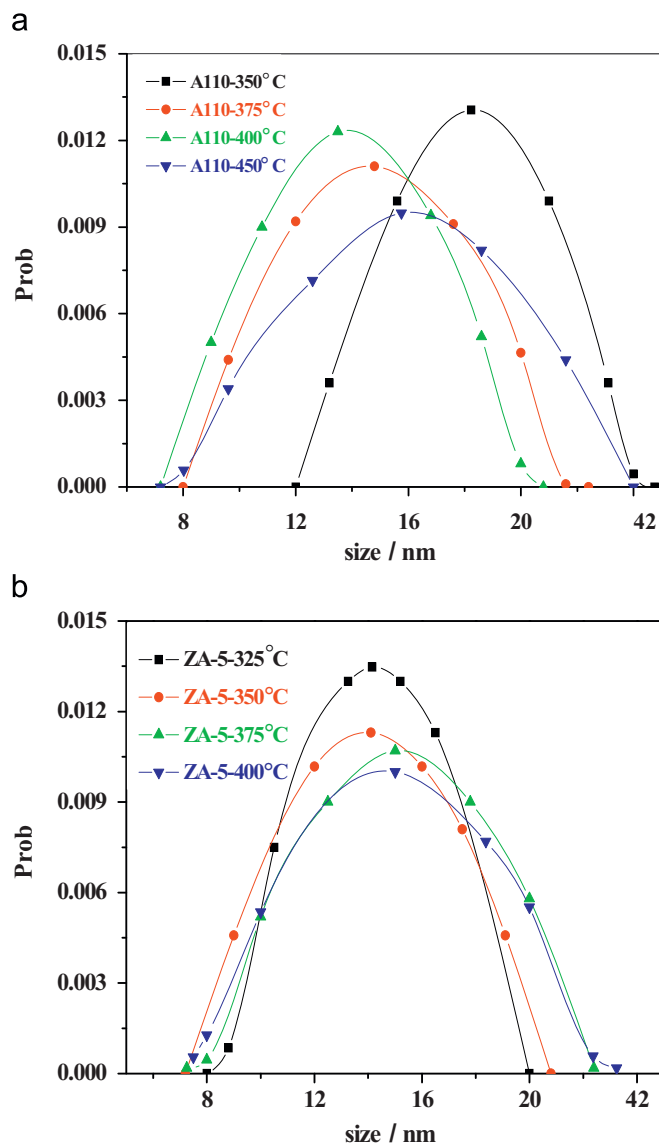
ZA-5 catalyst might be related to the high concentrations of defect lattice of iron ion in wustite $Fe_{1-x}O$ precursor. During the coherent growth, the greater the lattice defect exists in the precursor, the larger the lattice microstrain is expected in the active phase α-Fe.

3.5. Simulation of the grain morphology of active phase α-Fe

Rietveld's whole profile fitting method based on crystal structure refinement is applied to extract the microstructure information of the reduced A110 and ZA-5 catalysts by using Software Maud 2.046. By the process of successive profile refinements the values of different structural and microstructural parameters in the simulated pattern are simultaneously modified to fit the experimental diffraction pattern. Fig. 9 shows the results of refinement analysis. The dots represent step-scanned experimental data and the continuous line through dots represents theoretical/simulated powder diffraction pattern. Residue of fitting data is shown at the bottom of the plot as (Io–Ic) where Io is the experimental data and Ic is the theoretical/simulated data points, respectively. The value indicates that the
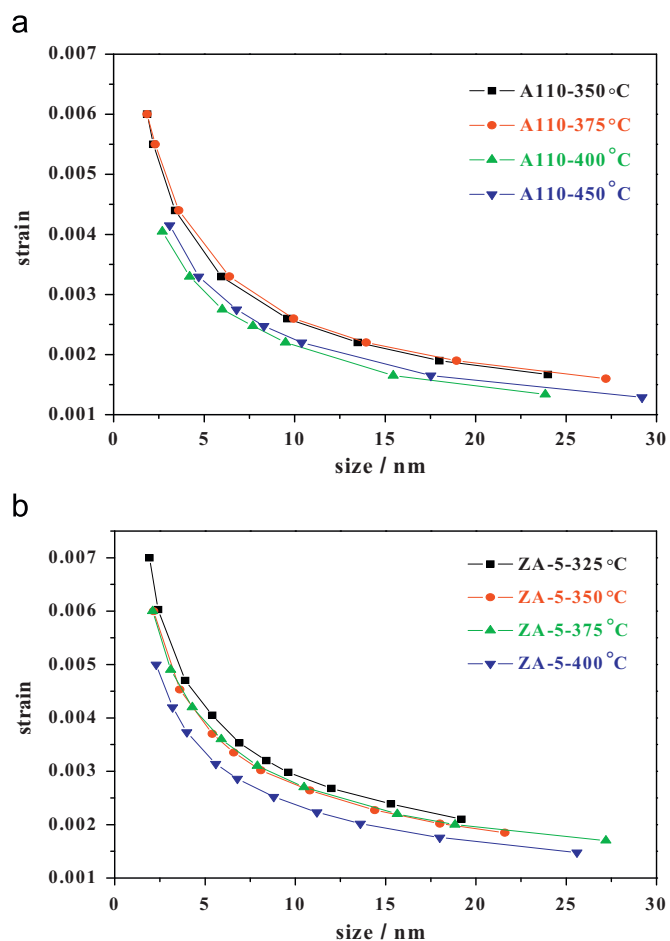
a

b

Fig. 8. Microstrain of active phase α-Fe at different reduction temperatures for (a) A110 and (b) ZA-5.

a

b

Fig. 9. The fitted results of all chart for A110 and ZA-5 catalysts.

fitting of the experimental data is successful (see Fig. 9). By using the fitted parameters and peak function, we have also simulated the grain morphology of active phase α-Fe on Popa model of the Software Maud 2.046 (see Fig. 10). As can be seen from Fig. 10, for A110 catalyst, the shape of active phase α-Fe grain looks like a concave cube, at which more (110) planes are exposed on the surface but less (111) and (211) planes are exposed. However, for ZA-5 catalyst, the grain of α-Fe has a mixed shape of cube and sphere with more exposed (111) and (211) planes but less exposed (110) plane.

3.6. HRTRM observations

To observe the microstructure of the formed α-Fe, we have used HRTEM to examine the catalyst after reduction. The size distribution range measured by HRTEM is about 10–15 nm, according with the average grain size calculated by Warren–A-verbach's method. Fig. 11 shows a typical image found in the ZA-5 catalyst after reduction at 450 °C in the *in situ* experiment. A measurement finds that the lattice spacing of the observed crystallite is about 0.201 nm, in good agreement with that of Fe(110) ($d = 0.20268$ nm). It is also found that this particle seems to consist of two parts, namely an outer shell and an interior. However, there is no difference between the lattice spacings of the two parts, indicating that this particle is completely reduced.
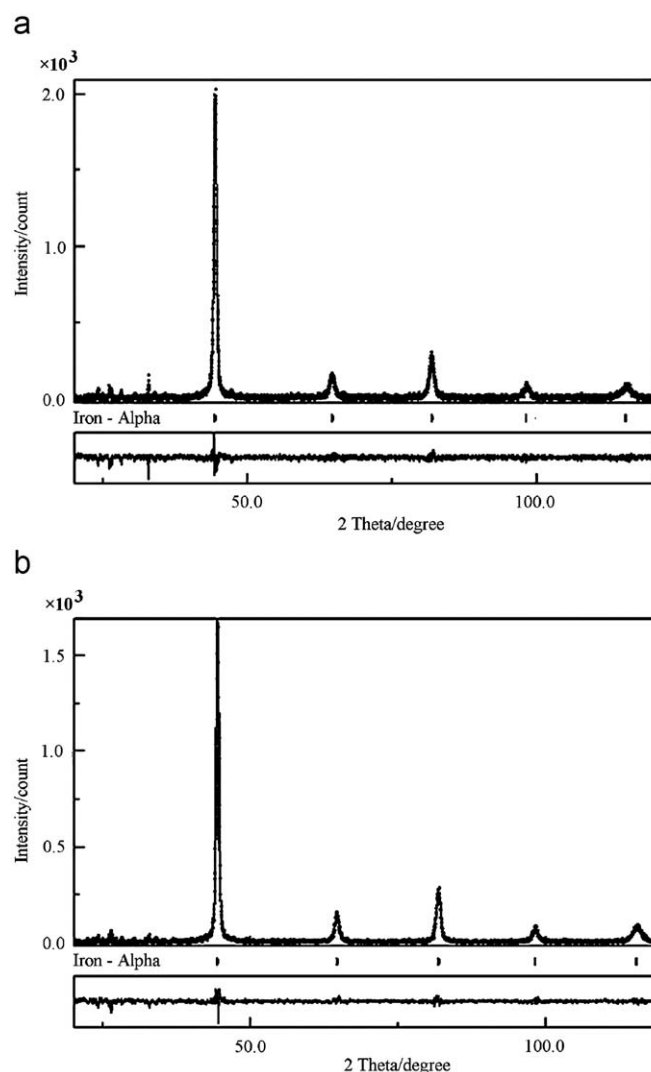
4. Discussion

4.1. Reduction model of Fe_3O_4 and $Fe_{1-x}O$ catalysts

The *in situ* XRD results, as well as HRTEM observations, have shown that during the temperature-programmed reduction the active phase of α-Fe exhibits several abnormal growth features. (i) The average grain size decreases with temperature at the beginning of reduction. After that, the grain sizes keep relatively stability before sintering. (ii) Larger microstrain is generally observed at the beginning of reduction and decreases with increasing temperature. (iii) The number of crystallite grain shows an increasing trend with temperature. (iv) The distribution of grain size becomes wider with increasing temperature. Based on the above observations, we propose the following model for the growth of α-Fe during catalyst reduction (see Fig. 12). First, reduction starts from outside of the aggregated oxide particles (namely precursor). Because there exist pores between the aggregated oxide particles, H_2 can diffuse into the pores, and thus reduction may also occur inside the precursor simultaneously. Consequently, a "microcrystalline film" forms. The observation of larger average grain size at the beginning of reduction might be related to the shrinkage of the oxides to metal during reduction. In addition, the lattice mismatch between the
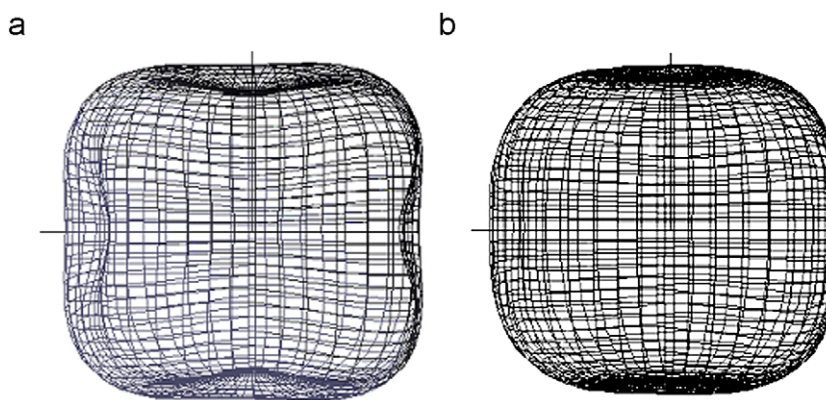
Fig. 10. The simulated grain morphology of the active phase α-Fe based on the XRD patterns of reduced catalysts: (a) A110 catalyst and (d) ZA-5 catalyst.

precursor and the formed active phase "film" will produce large lattice distortion, namely microstrain, during reduction [23]. Secondly, as the temperature increases and the reduction continues, the stress at the coherent interface between the precursor and thickening microcrystalline film of α-Fe will decreases. Moreover, the continuingly shrinking of these oxide particles may result in the breaking of the aggregated oxide particle, and thus forms smaller grains. Thirdly, the generated smaller grains are further reduced by H_2. As mentioned above, due to the presence of the exsolution products, released from the structure promoters, segregate to grain boundary, the growth of these smaller grains is hindered till the temperature is high enough to cause sintering.

4.2. Origins for the activity difference between ZA-5 and A110 catalysts

Based on our above experimental and simulated results, the possible origins for the activity difference between ZA-5 and A110 catalysts are given as follows. (i) The $Fe_{1-x}O$-based catalyst ZA-5 has a lower reduction temperature and a faster reduction rate than Fe_3O_4-based catalyst A110. In other words, a higher degree of reduction can be obtained for ZA-5 at lower reduction temperature and at short time and thus lead to higher activity in comparison to A110. (ii) It is believed that the (111) and (211) planes are the crystallographic planes of high catalytic activity in ammonia-synthesis [24]. Thus, our simulated result that the active phase α-Fe of the ZA-5 catalyst owns more exposing (111) and (211) planes than that of the A110 catalyst can serve as another reason for the higher activity observed in the ZA-5 catalyst. (iii) α-Fe of the ZA-5 catalyst possesses a higher microstrain than that of the A110 catalyst. In general, the higher lattice microstrain indicates more defects on the surface that can serve as active sites for chemical reaction and thus results in higher catalytic activity, which has also been observed in Cu catalysts [25,26].

5. Conclusion

We have presented an *in situ* XRD investigation of the temperature-programmed reduction processes of two types of industrial ammonia-synthesis catalysts, $Fe_{1-x}O$-based ZA-5 and Fe_3O_4-based A110. Several results have been obtained from our experimental and simulated results: (i) the $Fe_{1-x}O$-based catalyst ZA-5 has a lower reduction temperature and a faster reduction rate than Fe_3O_4-based catalyst A110; (ii) for A110 catalyst the shape of active phase α-Fe grain looks like a concave cube, at which more (110) plane is exposed on the surface but less (111) and (211) planes are exposed. However, for ZA-5 catalyst, the grain
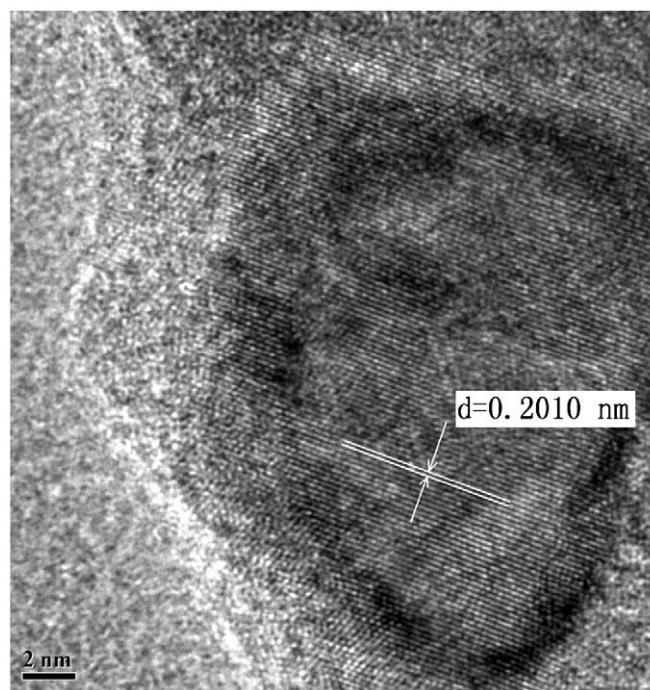

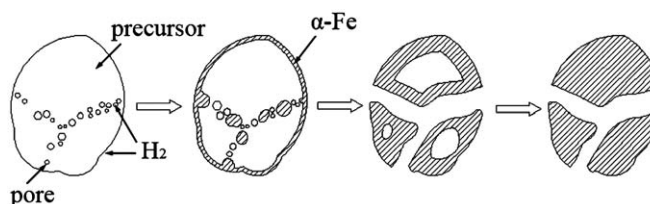**Fig. 11.** HRTEM image of an α-Fe particle.

Fig. 12. A proposed growth model of active phase α-Fe during reduction.

of active phase α-Fe has a mixed shape of cube and sphere with more exposed (111) and (211) planes but less exposed (110) plane; (iii) the active phase α-Fe of ZA-5 catalyst in general possesses a higher value of lattice microstrain than that of A110 catalyst. These differences serve as the possible origins for the activity difference between two types of catalysts. Based on the XRD results, as well as the observations by HRTEM, a model is also proposed to describe the growth of α-Fe during the reduction of Fe_3O_4- and $Fe_{1-x}O$-based ammonia-synthesis catalysts.

Acknowledgments

References

[1] N. Pernicone, F. Ferrero, I. Rossetti, L. Forni, P. Canton, P. Riello, G. Fagherazzi, M. Signoretto, F. Pinna, Appl. Catal. A 251 (2003) 121.
[2] Z. Lendzion-Bielun, Pol. J. Chem. 81 (2007) 433.
[3] W. Arabczyk, I. Jasinska, K. Lubkowski, React. Kinet. Catal. Lett. 83 (2004) 385.
[4] M.J. Figurski, W. Arabczyk, Z. Lendzion-Bielun, R.J. Kalenczuk, S. Lenart, Appl. Catal. A 247 (2003) 9.
[5] S. Natesakhawat, X.Q. Wang, L.Z. Zhang, U.S. Ozkan, J. Mol. Catal. A 260 (2006) 82.
[6] M. Ding, Y. Yang, B. Wu, J. Xu, C. Zhang, H. Xiang, Y. Li, J. Mol. Catal. A (2008) doi:10.1016/j.molcata.2008.12.016.
[7] G. Fagherazzi, F. Galante, F. Garbassi, N. Pernicone, J. Catal. 26 (1972) 344.
[8] US Patent 5, 846, 507, 1996; European Patent 0,763,379, 2002; and Germany Patent 69430143T2, 2002.
[9] Z. Lendzion-Bieluň, W. Arabczyk, M. Figurski., Appl. Catal. A (2002) 255.
[10] H.Z. Liu, X.N. Li, Ind. Eng. Chem. Res. 36 (1997) 335.
[11] H.Z. Liu, X.N. Li, Z.N. Hu, J. Appl. Catal. A 142 (1996) 209.
[12] H.Z. Liu, Chin. J. Catal. 22 (2001) 304.
[13] B. Herzog, D. Herein, R. Schlögl, Appl. Catal. A 141 (1996) 71.
[14] H. Natter, M. Schmelzer, M.S. Löffler, C.E. Krill, A. Fitch, R. Hempelmann, J. Phys. Chem. B 104 (2000) 2467.
[15] P. Bose, S.K. Pradhan, S. Sen, Mater. Chem. Phys. 80 (2003) 73.
[16] T. Selcan, G.R. Jean, S. Cristina, B. Jean-Louis, C. Bernard, G. Etienne, H. Rolf-Dieter, C.R. Ute, P. Rainer, J. Solid State Chem. 182 (2009) 229.
[17] A.L. Ortiz, L. Show, Acta Mater. 52 (2004) 2185.
[18] A. Kremenovic, B. Antic, V. Spasojevic, M. Vucinic-Vasic, Z. Jaglicic, J. Prinat, Z. Trontelg, J. Phys: Condens. Matter 17 (2005) 4285.
[19] N.C. Popa, J. Appl. Crystallogr. 31 (1998) 176.
[20] N.C. Popa, J. Appl. Crystallogr. 25 (1992) 611.
[21] H.Z. Liu, Chin. J. Catal. 22 (2001) 304.
[22] G.F. Luo, Treatise in Crystograph, Geology Publishing Company, Beijing, 1985 pp. 71–73.
[23] Y.H. Wang, The Foundation of X-ray Diffraction, Atomic Publishing Company, Beijing, 1985 pp. 258–262.
[24] G.A. Somorjai, N. Materer, Top. Catal. 1 (1994) 215.
[25] K.C. Waugh, Catal. Lett. 58 (1999) 163.
[26] M. Kurtz, H. Wilmer, T. Genger, O. Hinrichsen, M. Muhler, Catal. Lett. 86 (2003) 77.